

Generation of Terahertz Radiation from Fe-doped InGaAsP Using 800 nm to 1550 nm Pulsed Laser Excitation

O. Hatem^{1,2} · J. R. Freeman¹ · J. E. Cunningham¹ · P. J. Cannard³ · M. J. Robertson³ · E. H. Linfield¹ · A. G. Davies¹ · D. G. Moodie³

Received: 17 September 2015 / Accepted: 30 November 2015 /

Published online: 22 December 2015

© The Author(s) 2015. This article is published with open access at Springerlink.com

Abstract We demonstrate efficient generation of terahertz (THz) frequency radiation by pulsed excitation, at wavelengths between 800 and 1550 nm, of photoconductive (PC) switches fabricated using Fe-doped InGaAsP wafers, grown by metal organic chemical vapor deposition (MOCVD). Compared to our previous studies of Fe-doped InGaAs wafers, Fe:InGaAsP wafers exhibited five times greater dark resistivity to give a value of 10 k Ω cm, and Fe:InGaAsP PC switches produced five times higher THz power emission. The effect of Fe-doping concentration (between 1E16 and 1.5E17 cm⁻³) on optical light absorption (between 800 and 1600 nm), on resistivity, and on THz emission is also discussed.

Keywords Terahertz waves · Photo-emission · Photoconductive switches · Fe:InGaAsP · Fe:InGaAs · MOCVD

1 Introduction

Over the recent years, there have been an increasing number of applications for terahertz (THz) frequency (0.1–10 THz) waves, including their use in medical imaging [1–3], security scanning [4–6], and the analysis of pharmaceutical compounds [7, 8]. This has stimulated the need for developing robust, compact, and cheap THz instrumentation. Having high excitation power (>0.5 W at 800 nm) for efficient THz generation from large-aperture LT-GaAs photoconductive (PC) emitters (the most efficient photoconductive material for THz emission at 800 nm due to its high resistivity >10⁵ Ω cm and its subpicosecond carrier lifetime) would not be possible without

✉ O. Hatem
osama.e.hatem@gmail.com

¹ School of Electronic and Electrical Engineering, University of Leeds, Leeds LS2 9JT, UK

² Department of Engineering Physics and Mathematics, Faculty of Engineering, Tanta University, Tanta, PO Box 31521, Egypt

³ CIP Technologies, Adastral Park, Martlesham Heath, Ipswich Suffolk IP5 3RE, UK

using complex and expensive Ti:sapphire lasers. Relatively compact and cheap fiber lasers centered at 1550 nm would be a good replacement if appropriate photoconductive materials with suitable optical and electrical characteristics could be found for THz generation and detection at this wavelength. Indium gallium arsenide ($\text{In}_x\text{Ga}_{x-1}\text{As}$) has been the first choice for many research groups as its band-gap can be easily tailored to match the photon energy at 1550 nm by changing the growth ratio between In and Ga atoms. However, its low dark resistivity produces significant problems in its use for PC THz emitters and detectors. Devices with high resistivity can withstand high external electric bias field for enhanced THz emission and make the devices less sensitive to external noise when used as PC detectors. Introducing defects into InGaAs crystal by Fe implantation [9], Br^+ ion irradiation [10], and Be-doping [11] has shown some success in enhancing the resistivity to 0.63, 5, and 700 Ω cm, respectively. More complex structures have also been investigated; an ErAs/InGaAs superlattice structure showed a resistivity of 343 Ω cm [12], while a Be-InGaAs/InAlAs superlattice structure achieved a maximum sheet resistance of 1E6 Ω /sq (200 Ω cm dark resistivity) [13, 14]. Fe-implanted InGaAsP has also been investigated, showing a maximum resistivity of 2.5 k Ω cm [15, 16].

Recently, we investigated THz emission and detection using Fe-doped $\text{In}_{0.53}\text{Ga}_{0.47}\text{As}$ [17–19]. While being able to use this material (at different Fe-doping concentrations) in the generation and detection of THz waves, its 2.2 k Ω cm maximum achieved dark resistivity (2.2E7 Ω /sq sheet resistance) limited its use for PC THz emitters to <3 and <15 kV/cm of DC and AC electric bias fields, respectively (at an incident optical fluence of 40 $\mu\text{J}/\text{cm}^2$). We note that the maximum resistivity that can be achieved from Fe-doped InGaAs was theoretically estimated to be 4 k Ω cm [20]. The maximum THz emission power that we measured from Fe-InGaAs PC emitter was ~ 10 μW (200 mW peak power if a THz pulse width of 0.5 ps is assumed).

In this paper, we report the use of epitaxially grown Fe-doped InGaAsP as a photoconductive material; this has advantages over Fe-implanted InGaAsP materials, including better control over the Fe compensator distribution while producing less damage to the crystal structure. These materials show significant improvements in their photonic and electrical characteristics compared with the ternary, epitaxially grown, Fe-doped $\text{In}_{0.53}\text{Ga}_{0.47}\text{As}$ materials that we previously studied. We investigate systematically the effect of changing the Fe-doping concentration on the optical absorption, resistivities, and the emitted THz power from Fe-doped InGaAsP wafers. In comparison with Fe-doped $\text{In}_{0.53}\text{Ga}_{0.47}\text{As}$, we observe an enhanced surface homogeneity, and an increased wafer resistivity by a factor of five (to give a value of 10 k Ω cm), and increased THz power emission by a factor of five (~ 50 μW average power). We also directly compare the performance at 800 nm with emitters fabricated with identical electrode geometry on Fe: $\text{In}_{0.53}\text{Ga}_{0.47}\text{As}$ semiconductors.

2 Experimental Study

2.1 Growth Details of Fe-doped InGaAsP Wafers

The layer structure of our lattice-matched Fe:InGaAsP wafers is shown in Fig. 1a. The atomic fractions of the wafer constituents (Fe: $\text{In}_{0.70}\text{Ga}_{0.30}\text{As}_{0.87}\text{P}_{0.13}$) were chosen to give a band-gap energy of 0.8 eV [21] to enable light absorption up to a wavelength of 1550 nm. The band-gap spectra around 1550 nm were confirmed with photoluminescence (PL) measurements, as shown in Fig. 1b. The metal organic chemical vapor deposition (MOCVD) growth was conducted at 810 torr (1065 mbar) pressure and 660 $^\circ\text{C}$ (thermocouple) growth temperature

in a horizontal quartz reactor. Before each growth, the susceptor and reactor were conditioned using a baking and cleaning procedure to ensure reproducible starting conditions. The precursors used were trimethylindium (TMI), trimethylgallium (TMG), 100 % arsine (AsH_3), and 100 % phosphine (PH_3) as the sources for In, Ga, As, and P atoms, respectively. Ferrocene ($\text{Fe}(\text{C}_5\text{H}_5)_2$) from a sublimation bubbler was used as the iron dopant source. All precursors were semiconductor grade (or better). Purified H_2 was used as the carrier gas, and the total gas flow through the reactor during epitaxy was $\sim 115 \text{ cm}^3/\text{s}$. Bubbler pickups, dilution, and pusher flows were also H_2 . Wafer growth was terminated by an n-doped InP encapsulation layer to avoid having an As-terminated surface (the volatility of As would have been detrimental if post-growth annealing had been required). Fe doping was undertaken uniformly, with the doping level being changed systematically between different wafers. The Fe doping allowed compensation of the residual n-type carriers in the InGaAsP, increasing the resistance of the material, as well as providing mid-gap states, which act to rapidly capture the photogenerated carriers. All MOCVD crystal growths were undertaken on 50-mm diameter, (100) oriented, Fe-doped InP substrates. Quaternary layers were grown with a reproducible rate of $7.24 \text{ }\mu\text{m}/\text{h}$, and InP buffers/caps were grown at a rate of $3 \text{ }\mu\text{m}/\text{h}$. Secondary ion mass spectroscopy (SIMS) analysis for each wafer showed a uniform doping density throughout the thicknesses of the Fe:InGaAsP layers.

Optical Nomarski pictures with a X20 objective showed defect-free specular surfaces, indicating a homogenous morphology. The surface morphologies were smoother than those obtained from the equivalent Fe:InGaAs ternary structures, where there was some evidence of FeAs precipitates on the surfaces. The high quality of the surface reflects the fact that the quaternary composition is well-matched to the InP substrate. To improve the surface quality of Fe:InGaAs wafers, N_2 may be used as the carrier gas during growth instead of H_2 [22–24].

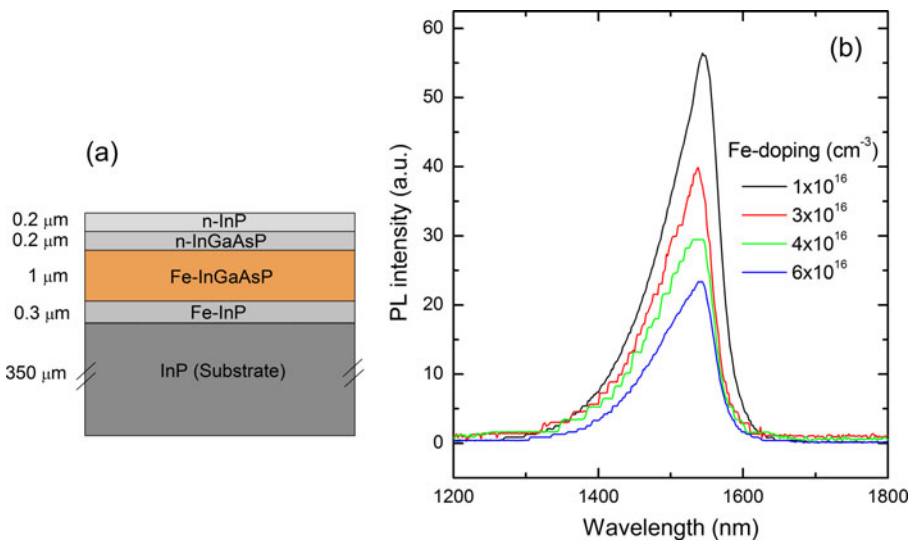


Fig. 1 a The layer structure for the MOCVD Fe:InGaAsP wafers used in this study and (b) the photoluminescence intensity from different Fe-doped InGaAsP wafers (signals are arbitrarily scaled for clarity)

2.2 Details of PC Emitters and THz Characterization Systems

Bow-tie PC THz emitters (comprising two 8-mm long electrodes, with a 300- μm gap between electrodes) were fabricated by photolithography, on several different Fe-doped InGaAsP wafers. First, the n-InP cap layer was chemically etched in HCl for 20 s, and then the n-InGaAsP layer was etched in 100:10:10 (by volume) $\text{H}_2\text{O}:\text{H}_2\text{O}_2:\text{H}_2\text{SO}_4$ for 40 s to expose the Fe:InGaAsP surface. Finally, metal electrodes (20 nm Ti/150 nm Au) were deposited on top of the exposed Fe:InGaAsP layer.

THz emission at 1550 nm excitation was first demonstrated using a THz-TDS system based on a fiber laser (Pro-NIR, Toptica) with a <100 fs pulse width (Fig. 2). The output beam at 1550 nm was split into two paths using a beam splitter. A pump beam (80 mW average power) was mechanically chopped at 2.8 kHz and guided by mirrors to excite the gap between the electrodes of a PC emitter, while the probe beam (40 mW) was guided onto a 1-mm thick ZnTe crystal to probe the collinearly incident THz radiation using electro-optic sampling. The emitter electrodes were DC-biased at 50 V. The polarization components of the probe beam were separated after passing through the ZnTe crystal by a quarter wave plate and Wollaston prism, and their respective intensities then measured using a pair of balanced photodiodes connected to a lock-in amplifier, itself referenced to the modulating frequency of the mechanical chopper. The PC emitters were also tested at different excitation wavelengths (1150–1550 nm) using a Ti:sapphire-pumped optical parametric oscillator (OPO, Coherent) system as described elsewhere. Finally, the PC Fe:InGaAsP emitter with the highest radiated THz emission was compared to both Fe:InGaAs and conventional LT-GaAs emitters at an 800-nm excitation using a Ti:sapphire-based THz-TDS system (<100 fs, Tsunami, Spectra Physics).

3 Results and Discussions

3.1 Broadband Light Absorption and THz Emission at 1550-nm Excitation

Absorption of light from 800 nm to 1600 nm was clearly observed in the Fe:InGaAsP samples, as shown in Fig. 3a. Light (from a tungsten-halogen lamp) was shone onto the Fe-doped

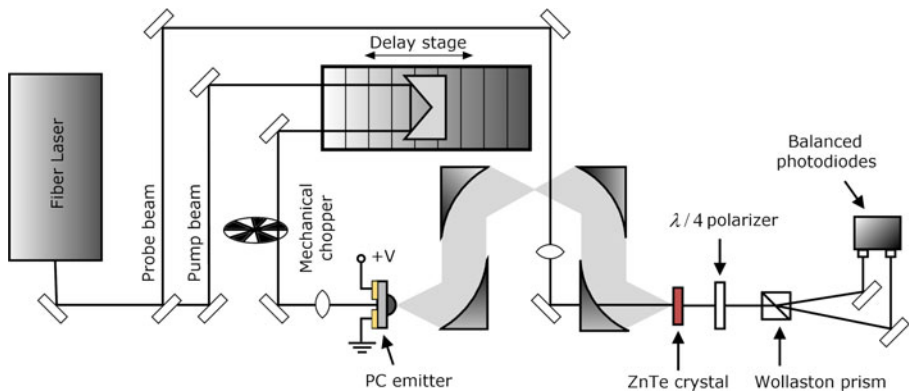


Fig. 2 THz-TDS system using a 1550-nm fiber laser system (providing <100 fs laser pulses, at an 80-MHz repetition rate) to pump PC Fe:InGaAsP emitters for THz generation. The THz radiation is probed by electro-optic sampling using 40 mW probe power at 1550 nm in a 1-mm thick ZnTe crystal

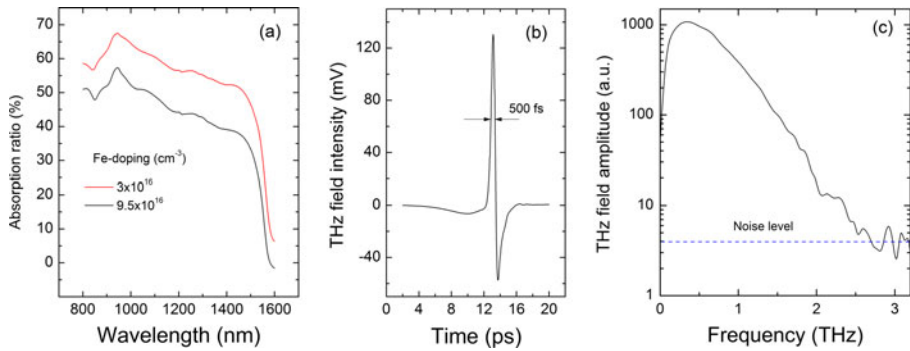


Fig. 3 **a** Ratios of the absorbed light by Fe:InGaAsP wafers between 800 nm and 1600 nm. **b** Time domain and **c** Fourier frequency transform signals for the THz radiation generated from a 7×10^{16} - cm^{-3} Fe-doped InGaAsP emitter at a 1550-nm excitation wavelength using a constant 80-mW pump power and a 50-V bias voltage

InGaAsP wafers, and the power intensity of the transmitted and reflected spectrums was measured using a grating spectrometer (Princeton instruments). The ratio of the absorbed power was then deduced by subtracting the transmitted and the reflected power fractions from the incident light power. As expected, the wafer with the higher doping concentration absorbed less power of the incident light, as the absorption coefficient is directly proportional to the conductivity of the material, and therefore, less incident power is absorbed with increasing conductivity [25].

An Fe:InGaAsP PC emitter (7×10^{16} cm^{-3} Fe doping) was tested for THz emission at 1550-nm excitation wavelength on the THz-TDS system shown in Fig. 2. Figure 3b, c shows the THz time-domain signal and the corresponding Fourier frequency transform (FFT) generated from the 7×10^{16} cm^{-3} Fe-doped InGaAsP PC emitter. The full width at half maximum of the time-domain signal (500 fs) reflects the fast dynamics of the photo-generated carriers in the emitter. The FFT signal shows frequency components up to 2.7 THz before the noise floor, with a signal to noise ratio (SNR) of >250:1 in amplitude at 0.5 THz.

3.2 Dependence of Integrated THz Power and Resistivities on Doping Concentrations

Figure 4a shows the integrated THz power (\sim the integral of the area under the square of the THz amplitude signal) of the emitted radiation at a 1550-nm excitation wavelength for Fe-doped InGaAsP emitters with different doping concentrations compared to similar results obtained from Fe-doped InGaAs emitters. Increasing the Fe doping led initially to an increase in the emitted THz power, until a peak was reached (at Fe concentrations of 7×10^{16} and 3×10^{16} cm^{-3} for Fe:InGaAsP and Fe:InGaAs, respectively). The emitted THz power then dropped for higher Fe-doping levels. This behavior may be explained in qualitative terms as follows: by increasing the Fe-doping level in the wafers, more trap centers are created for the photo-generated carriers, leading to fast capture and enhanced THz emission. However, increasing the density of Fe trap centers further leads to increased carrier scattering, a reduction in carrier mobility [25, 26], a reduction in light absorption (Fig. 3a), and hence, the observed reduction in output power.

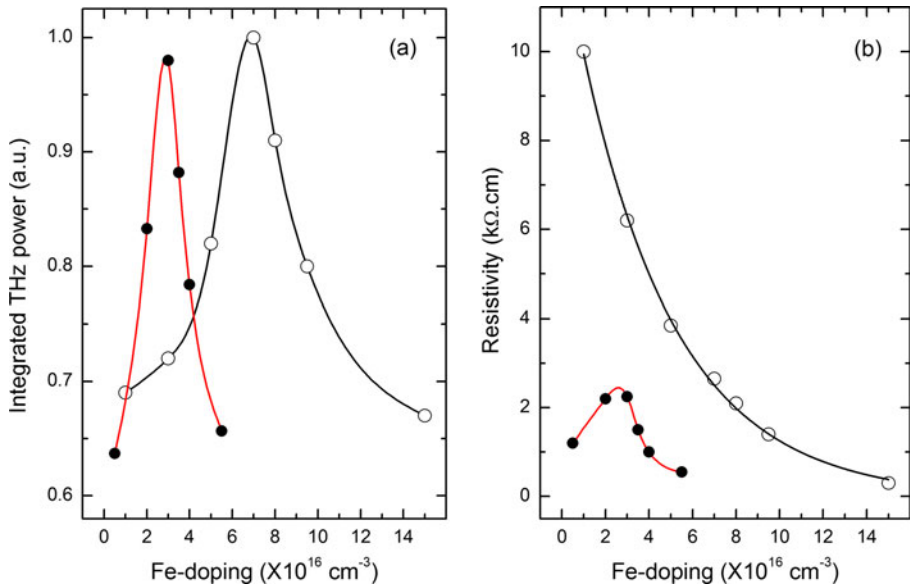


Fig. 4 **a** Integrated THz power of the THz radiation emitted from PC emitters made from several differently Fe-doped InGaAsP (hollow circles) and Fe-doped InGaAs (filled circles) wafers at a 1550-nm excitation wavelength measured with a constant 80-mW pump power and 50-V bias voltage. **b** The resistivity of different Fe-doped InGaAsP wafers (hollow circles) and Fe-doped InGaAs (filled circles) measured from Hall bar devices. The lines are guides to the eye

The resistivities of the Fe:InGaAsP and Fe:InGaAs samples were also determined from the I-V characteristics of at least two devices fabricated from each wafer into Hall bar geometries (variation in resistivity was found to be $<5\%$ between the two devices). The maximum resistivity for the Fe-doped InGaAsP wafer was about five times higher than that in the Fe:InGaAs materials (Fig. 4b), with the value of $10 \text{ k}\Omega \cdot \text{cm}$ (at $1 \times 10^{16} \text{ cm}^{-3}$ Fe doping) being the highest reported resistivity for a material emitting THz radiation at 1550 nm. In general, provided photocurrent is sustained, having high resistivity enables a greater bias voltage to be applied to the emitter electrodes without breakdown occurring, and hence, high power THz emission can be obtained. We note that some difficulties were found in measuring the mobility of the charge carriers in our materials using Hall bar devices under magnetic fields. We think these difficulties arise from some magnetization interactions with the Fe doping.

Although the principal reason for Fe doping the InGaAsP and InGaAs wafers was to increase the resistivity of the wafers by compensating the residual background conduction in the material, we noticed that increasing the Fe-doping level from 1×10^{16} to $1.5 \times 10^{17} \text{ cm}^{-3}$ in Fe:InGaAsP wafers actually resulted in a reduction in resistivity from 10 to $0.5 \text{ k}\Omega \cdot \text{cm}$. This implies that the wafers were becoming progressively more overcompensated, leading to p-type conduction. In contrast, for the Fe:InGaAs wafers, a maximum in resistivity was seen. This implied that the material changed from n-type to p-type, with full compensation being obtained at $\sim 2.5 \times 10^{16} \text{ cm}^{-3}$ Fe doping, where a maximum resistivity of $\sim 2.5 \text{ k}\Omega \cdot \text{cm}$ is observed, while noting that the maximum resistivity that could be obtained from a lattice-matched Fe:InGaAs wafer has been theoretically estimated to be $4 \text{ k}\Omega \cdot \text{cm}$ [20]. We also noticed a reversal in polarity for the THz time-domain signals emitted from the p-type and n-type Fe-InGaAs emitters which was another indication to the change of the material type.

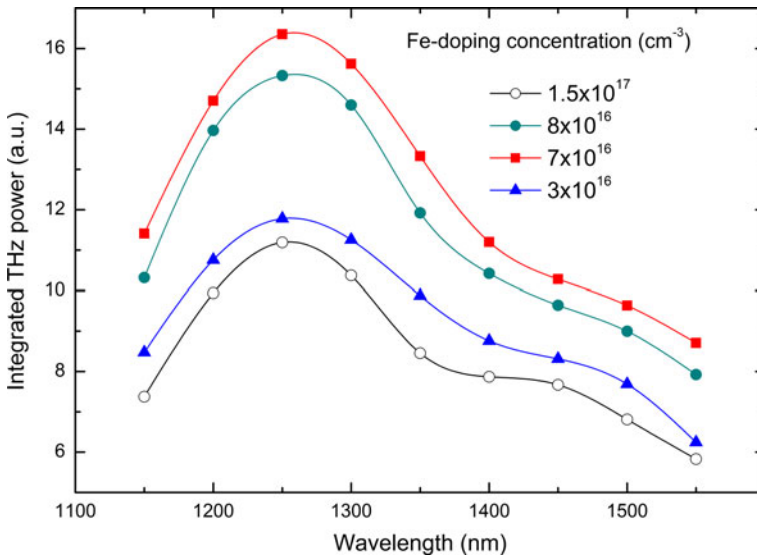


Fig. 5 Integrated power of the THz signals generated from different Fe-doped InGaAsP emitters excited with 50-mW pump power, and a 50-V-DC bias, at wavelengths from 1150 nm to 1550 nm. Lines are guides to the eye

Figure 5 shows the integrated power of the THz signals emitted from different Fe-doped InGaAsP emitters when excited with 50 mW average power at laser wavelengths varying from 1150 to 1550 nm, with the pump beam mechanically chopped at 2.8 kHz and the emitters biased with 50 V DC. The Fe:InGaAsP shows excellent capability for terahertz emission over a wide range of excitation wavelengths from 1150 to 1550 nm.

3.3 Dependence of THz Emission on Bias Voltage and Pump Power

To assess the Fe:InGaAsP emitters further, two emitters with different Fe-doping levels (1×10^{16} and 7×10^{16} cm^{-3}) were tested both at different DC bias voltages between 0–120 V (with the pump power of the 1550 nm excitation kept constant at 50 mW), and at different pump powers between 0–80 mW (with the DC bias voltage kept constant at 50 V), as shown in Fig. 6. The integrated THz power was found to follow a quadratic relationship with both the bias voltage and the pump power, in keeping with the standard theory of photoconductive emission [27, 28]. The highest power Fe:InGaAs emitter (doped at 3×10^{16} cm^{-3}) showed a performance comparable to that of the 7×10^{16} - cm^{-3} Fe-doped InGaAsP emitter up to a bias of 50 V, but then showed a saturation behavior. We attribute this saturation to the increased temperature of the substrate, due to the applied DC voltage, which causes much heat dissipation and a reduction in the carriers' mobility as a consequence. We note that one possible solution to avoid this saturation effect would be to use a fast alternating bias voltage waveforms with short duty cycle [18]. In contrast, the Fe:InGaAsP emitters continued to show THz emission at bias voltages beyond 100 V as a consequence of their increased resistivities. The emitter with the highest resistivity (at 1×10^{16} cm^{-3} Fe-doping level) withstood DC electric bias fields up to 12.5 kV/cm (at optical fluence of 40 $\mu\text{J}/\text{cm}^2$) and produced ~ 50 μW average THz emission power (measured using a helium-cooled bolometer). Using

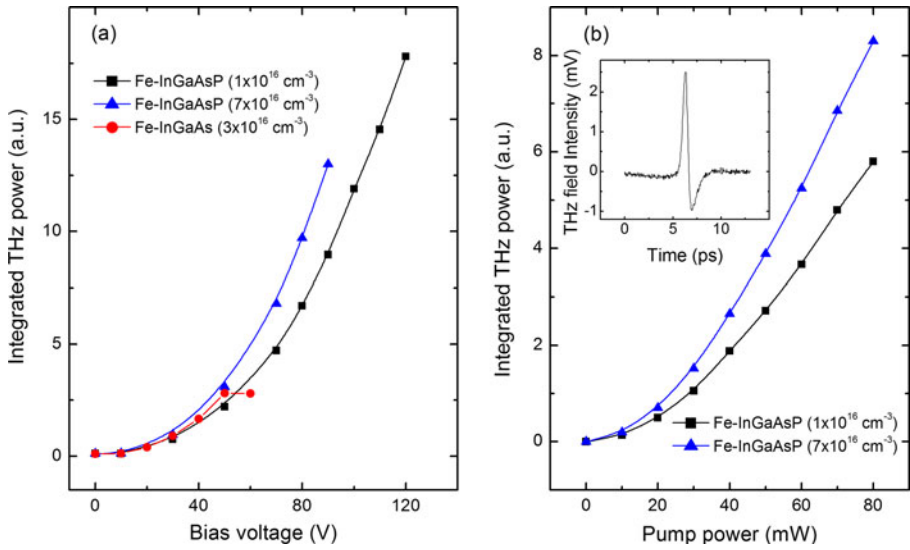


Fig. 6 **a** Integrated power of the emitted THz radiation from Fe-doped InGaAsP and Fe-InGaAs PC emitters using a constant 50-mW pump power at a 1550-nm wavelength and different bias voltages. **b** Integrated power of the emitted THz radiation from Fe-doped InGaAsP PC emitters using a constant 50-V bias voltage and different pump powers at a 1550-nm wavelength. (Inset THz time-domain signal emitted using 1-mW pump power at a 1550-nm wavelength and a 50-V bias voltage, to excite a 7×10^{16} -cm⁻³ Fe-doped InGaAsP PC emitter)

fast AC bias fields with short duty cycles would decrease the heat dissipation in the device and increase the breakdown fields to several tens of kilovolts per centimeter, and hence, more emitted THz power could be obtained. Under optical excitation of $40 \mu\text{J}/\text{cm}^2$, Fe:InGaAsP was found to withstand AC bias fields up to 35 kV/cm before breakdown. It should be noted that THz emission was also realized at zero bias voltage, which we attributed due to the gradient of the photogenerated carriers at the excitation area [29].

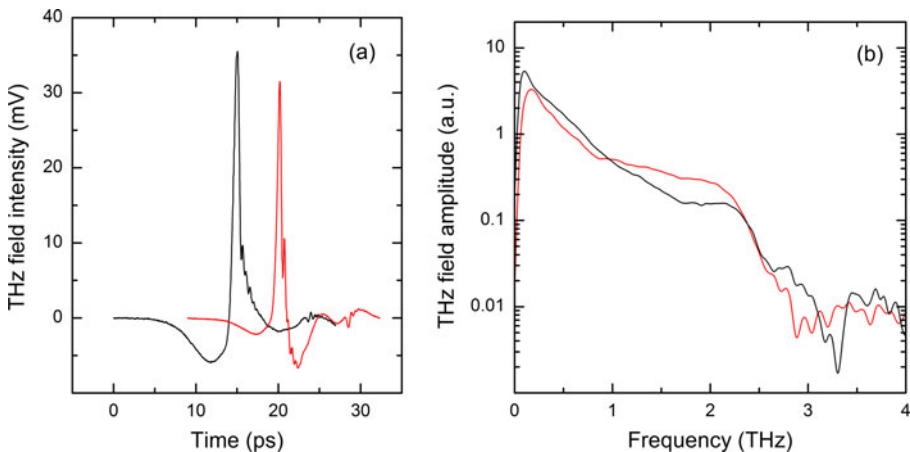


Fig. 7 **a** Time domain and **b** Fourier frequency transforms of the THz signals generated from 7×10^{16} cm⁻³ Fe-doped InGaAsP (black), 2×10^{16} cm⁻³ Fe-doped InGaAs (red) emitters with a 100-mW pump power, at an 800-nm excitation wavelength and using a 50-V bias voltage

Figure 6b (inset) shows a THz time-domain signal recorded from the $7 \times 10^{16} \text{ cm}^{-3}$ Fe-doped InGaAsP emitter (300 μm gap) at a 50-V bias, when it was excited with only 1 mW average laser power at 1550 nm. A signal-to-noise ratio of 20 (in amplitude) is obtained, indicating the promise of the material for use in on-chip THz devices at cryogenic temperature, where low excitation laser powers are essential (for example [30]).

3.4 THz Emission at 800 nm and Comparison with Fe:InGaAs

To evaluate further the emission from the Fe-doped InGaAsP material, a PC emitter ($7 \times 10^{16} \text{ cm}^{-3}$ Fe doping, 2.7 $\text{k}\Omega \text{ cm}$ resistivity) was also tested with an 800-nm excitation wavelength, and the results were compared directly with an Fe:InGaAs emitter ($3 \times 10^{16} \text{ cm}^{-3}$ doping). Both of these emitters used for comparison had the same electrode design and were tested under the same conditions of laser illumination and voltage bias (100 mW average laser power and 50 V DC bias). The Fe:InGaAsP emitter produced THz signals of amplitudes $\sim 10\%$ larger than that from the Fe:InGaAs emitter, as shown in Fig. 7. No higher test conditions were tried to avoid breaking the devices by the heating effects which could come from the high photon energies at 800 nm and/or higher DC bias fields. Fe:InGaAsP showed a higher bandwidth (~ 3.3 THz) at 800-nm excitation than that obtained at 1150–1550 nm excitations (Fig. 7b). This is likely to be a result of the longer coherence length (~ 2 mm) between the optical light at 800 nm and the incident THz radiation on the ZnTe detection crystal, while the coherence length is ~ 0.5 mm for optical light at 1550 nm for frequencies up to 4 THz [31, 32]. Further, we note that the shape of the THz signals generated from Fe:InGaAsP and Fe:InGaAs emitters changed by the excitation at 800 nm, which can be ascribed to the high photon energies at 800 nm.

4 Summary and Conclusions

In conclusion, MOCVD Fe:InGaAsP showed excellent performance as a THz source over a broad range of pulsed excitation wavelengths extending from 800 to 1550 nm. The Fe:InGaAsP wafers showed better surface homogeneity, high resistivities (up to 10 $\text{k}\Omega \text{ cm}$), and five times higher THz emission power ($\sim 50 \mu\text{W}$ average power) compared with our previous results from Fe:InGaAs.

Acknowledgements We acknowledge financial support from the EPSRC (UK) “COTS” program and the ERC grant “TOSCA”. AGD acknowledges support from the Royal Society and the Wolfson Foundation.

Open Access This article is distributed under the terms of the Creative Commons Attribution 4.0 International License (<http://creativecommons.org/licenses/by/4.0/>), which permits unrestricted use, distribution, and reproduction in any medium, provided you give appropriate credit to the original author(s) and the source, provide a link to the Creative Commons license, and indicate if changes were made.

References

1. D. Grischkowsky, S. Keiding, M. Vanexter, C. Fattinger, "Far-infrared time-domain spectroscopy with terahertz beams of dielectrics and semiconductors", *Journal of the Optical Society of America B-Optical Physics*, vol. 7, pp. 2006–2015, 1990.
2. B. B. Hu and M. C. Nuss, "Imaging with terahertz waves", *Optics Letters*, vol. 20, p. 1716, 1995.

3. D.M. Mittleman, M. Gupta, R. Neelamani, R.G. Baraniuk, J.V. Rudd, M. Koch, "Recent advances in terahertz imaging", *Applied Physics B-Lasers and Optics*, vol. 68, pp. 1085–1094, 1999.
4. W.H. Fan, A. Burnett, P.C. Upadhyaya, J. Cunningham, E.H. Linfield, A.G. Davies, "Far-infrared spectroscopic characterization of explosives for security applications using broadband terahertz time-domain spectroscopy", *Applied Spectroscopy*, vol. 61, pp. 638–643, 2007.
5. M. Walther, B.M. Fischer, A. Ortner, A. Bitzer, A. Thoman, H. Helm, "Chemical sensing and imaging with pulsed terahertz radiation", *Analytical and Bioanalytical Chemistry*, vol. 397, pp. 1009–1017, 2010.
6. J.F. Federici, B. Schulkin, F. Huang, D. Gary, R. Barat, F. Oliveira, D. Zimdars, "THz imaging and sensing for security applications - explosives, weapons and drugs", *Semiconductor Science and Technology*, vol. 20, pp. S266-S280, 2005.
7. V.P. Wallace, P.F. Taday, A.J. Fitzgerald, R.M. Woodward, J. Cluff, R.J. Pye, D.D. Arnone, "Terahertz pulsed imaging and spectroscopy for biomedical and pharmaceutical applications", *Faraday Discussions*, vol. 126, pp. 255–263, 2004.
8. J.A. Zeitler, P.F. Taday, D.A. Newnham, M. Pepper, K.C. Gordon, T. Rades, "Terahertz pulsed spectroscopy and imaging in the pharmaceutical setting - a review", *Journal of Pharmacy and Pharmacology*, vol. 59, pp. 209–223, 2007.
9. M. Suzuki and M. Tonouchi, "Fe-implanted InGaAs terahertz emitters for 1.56 μm wavelength excitation", *Applied Physics Letters*, vol. 86, p. 051104, 2005.
10. J. Mangeney and P. Crozat, "Ion-irradiated $\text{In}_{0.53}\text{Ga}_{0.47}\text{As}$ photoconductive antennas for THz generation and detection at 1.55 μm wavelength", *Comptes Rendus Physique*, vol. 9, pp. 142–152, 2008.
11. A. Takazato, M. Kamakura, T. Matsui, J. Kitagawa, Y. Kadoya, "Terahertz wave emission and detection using photoconductive antennas made on low-temperature-grown InGaAs with 1.56 μm pulse excitation", *Applied Physics Letters*, vol. 91, p. 3, 2007.
12. F. Ospald, D. Maryenko, K. von Klitzing, D.C. Driscoll, M.P. Hanson, H. Lu, A.C. Gossard, J.H. Smet, "1.55 μm ultrafast photoconductive switches based on ErAs : InGaAs", *Applied Physics Letters*, vol. 92, p. 131117, 2008.
13. B. Sartorius, H. Roehle, H. Kunzel, J. Bottcher, M. Schlak, D. Stanze, H. Venghaus, M. Schell, "All-fiber terahertz time-domain spectrometer operating at 1.5 μm telecom wavelengths", *Optics Express*, vol. 16, pp. 9565–9570, 2008.
14. H. Roehle, R.J.B. Dietz, H.J. Hensel, J. Bottcher, H. Kunzel, D. Stanze, M. Schell, B. Sartorius, "Next generation 1.5 μm terahertz antennas: mesa-structuring of InGaAs/InAlAs photoconductive layers", *Optics Express*, vol. 18, pp. 2296–2301, 2010.
15. A. Fekecs, M. Bernier, D. Morris, M. Chicoine, F. Schiettekatte, P. Charette, R. Ares, "Fabrication of high resistivity cold-implanted InGaAsP photoconductors for efficient pulsed terahertz devices", *Optical Materials Express*, vol. 1, pp. 1165–1177, 2011.
16. F. André, C. Martin, I. Bouraoui, S. François, G.C. Paul, A. Richard, "Towards semi-insulating InGaAsP/InP layers by post-growth processing using Fe ion implantation and rapid thermal annealing", *Journal of Physics D: Applied Physics*, vol. 46, p. 165106, 2013.
17. C.D. Wood, O. Hatem, J.E. Cunningham, E.H. Linfield, A.G. Davies, P.J. Cannard, D.G. Moodie, M. Pate, M.J. Robertson, "THz generation using 800 to 1550 nm excitation of photoconductors", *IEEE 34th International Conference on Infrared, Millimeter, and Terahertz Waves (IRMMW-THz 2009)*, pp. 1–3, 2009. doi: 10.1109/ICIMW.2009.5324613.
18. C.D. Wood, O. Hatem, J.E. Cunningham, E.H. Linfield, A.G. Davies, P.J. Cannard, M.J. Robertson, D.G. Moodie, "Terahertz emission from metal-organic chemical vapor deposition grown Fe:InGaAs using 830 nm to 1.55 μm excitation", *Applied Physics Letters*, vol. 96, p. 194104, 2010.
19. O. Hatem, J. Cunningham, E.H. Linfield, C.D. Wood, A.G. Davies, P.J. Cannard, M.J. Robertson, D.G. Moodie, "Terahertz-frequency photoconductive detectors fabricated from metal-organic chemical vapor deposition-grown Fe-doped InGaAs", *Applied Physics Letters*, vol. 98, p. 121107, 2011.
20. B. Tell, U. Koren, B.I. Miller, "Metalorganic vapor-phase-epitaxial growth of Fe-doped $\text{In}_{0.53}\text{Ga}_{0.47}\text{As}$ ", *Journal of Applied Physics*, vol. 61, p. 1172, 1987.
21. M. Silver and E. P. O'Reilly, "Optimization of long wavelength InGaAsP strained quantum-well lasers," *IEEE Journal of Quantum Electronics*, vol. 31, pp. 1193–1200, 1995.
22. M.P. H. Hardtdegen, H. Menhal, J.-T. Zettler, W. Richter, D. Schmitz, "In situ characterization of GaAs growth in nitrogen atmosphere during MOVPE- a comparison to hydrogen atmosphere", *Journal of Crystal Growth*, vol. 195, pp. 211–216, 1998.
23. M.H. Hilde Hardtdegen, R. Meyer, R. Carius, H. Münder, S. Frohnhoff, D. Szyuka, and H. Lüth, "MOVPE growth of GaAs using a N_2 carrier", *Journal of Crystal Growth*, vol. 124, pp. 420–426, 1992.
24. Y.S. Cho, H. Hardtdegen, N. Kaluza, N. Thilloßen, R. Steins, Z. Sofer, H. Lüth, "Effect of carrier gas on GaN epilayer characteristics", *Physica Status Solidi (C)*, vol. 3, pp. 1408–1411, 2006.
25. X. C. Zhang and D. H. Auston, "Optoelectronic measurement of semiconductor surfaces and interfaces with femtosecond optics", *Journal of Applied Physics*, vol. 71, p. 326, 1992.

26. D. Hahn, O. Jaschinski, H.-H. Wehmann, and A. Schlachetzki, "Electron-concentration dependence of absorption and refraction in n-In_{0.53}Ga_{0.47}As near the band-edge", *Journal of Electronic Materials*, vol. 24, p. 1357, 1995.
27. P.K. Benicewicz, J.P. Roberts, A.J. Taylor, "Scaling of terahertz radiation from large-aperture biased InP photoconductors", *Journal of the Optical Society of America B-Optical Physics*, vol. 11, pp. 2533–2546, 1994.
28. M.R. Stone, M. Naftaly, R.E. Miles, J.R. Fletcher, D.P. Steenson, "Electrical and radiation characteristics of semilarge photoconductive terahertz emitters", *IEEE Transactions on Microwave Theory and Techniques*, vol. 52, pp. 2420–2429, 2004.
29. R. Mueckstein, M. Natrella, O. Hatem, J.R. Freeman, C.S. Graham, C.C. Renaud, A.J. Seeds, E.H. Linfield, A.G. Davies, P.J. Cannard, M.J. Robertson, D.G. Moodie, O. Mitrofanov, "Near-field analysis of terahertz pulse generation from photo-excited charge density gradients", *IEEE Transactions on Terahertz Science and Technology*, vol. 5, pp. 260–7, 2015.
30. C.D. Wood, D. Mistry, L.H. Li, J.E. Cunningham, E.H. Linfield, A.G. Davies, "On-chip terahertz spectroscopic techniques for measuring mesoscopic quantum systems", *Review of Scientific Instruments*, vol. 84, p. 085101, 2013.
31. B. Pradarutti, G. Matthäus, S. Riehemann, G. Notni, S. Nolte, A. Tünnermann, "Highly efficient terahertz electro-optic sampling by material optimization at 1060 nm," *Optics Communications*, vol. 281, pp. 5031–5035, 2008.
32. N.C.J. van der Valk, P.C.M. Planken, A.N. Buijserd, H.J. Bakker, "Influence of pump wavelength and crystal length on the phase matching of optical rectification", *Journal of the Optical Society of America B-Optical Physics*, vol. 22, pp. 1714–1718, 2005.